




**Edge-passivation modulation of the transport properties in zigzag stanene nanoribbons**Yuan Li <sup>1,\*</sup>, Zhihui Chen,<sup>1</sup> Xiaolin Su,<sup>1</sup> Xinyu Cheng,<sup>1</sup> Yueyue Wang,<sup>1</sup> Gaofeng Xu <sup>1,†</sup> and Wu-Ming Liu <sup>2,‡</sup><sup>1</sup>*Department of Physics, Hangzhou Dianzi University, Hangzhou, Zhejiang 310018, China*<sup>2</sup>*Beijing National Laboratory for Condensed Matter Physics, Institute of Physics, Chinese Academy of Sciences, Beijing 100190, China*

(Received 27 September 2023; revised 18 May 2024; accepted 28 May 2024; published 13 June 2024)

We study the combined effect of the passivating atoms, edge electric fields, and exchange fields on the edge states, conductance, and spin polarization in zigzag stanene nanoribbons (ZSNRs). The distortion direction and amplitude of edge bands significantly depend on the electronegativity difference between the passivating atoms and tin atoms. The conductance dips can reflect the curved characteristic of the edge bands induced by passivating atoms, which can be used to detect the quantum spin-Hall edge states or passivating atoms. Interestingly, the edge antisymmetric electric fields can recover the passivation-induced band structures and transport properties, and an effective spin polarization can be realized by applying an exchange field on the edges of ZSNRs. The results provide a comprehensive understanding of the modulating method by utilizing the passivating atoms and the external fields, which will be of great help for the application of stanene devices.

DOI: [10.1103/PhysRevB.109.235414](https://doi.org/10.1103/PhysRevB.109.235414)**I. INTRODUCTION**

Topological insulators possess some electronic properties that can be employed in electronic devices such as topological field-effect transistors [1] and antiferromagnetic spintronics [2], which has triggered intensive interest in the fields of condensed matter physics. Stanene has a relatively larger band gap compared to other group IV counterparts like silicene and germanene [3], which can induce the quantum spin-Hall effect [4]. In 2015, ever since monolayers of stanene were successfully grown by molecular beam epitaxy on Bi<sub>2</sub>Te<sub>3</sub>(111) substrate [5], it has attracted great attention from researchers. The coexistence of topological edge states and superconductivity has been reported in stanene systems [6]. In addition, it is reported that stanene could achieve the anomalous quantum Hall effect [7] and dissipationless electron transport near room temperature [8,9], which is of great significance for the development of integrated electronics devices.

Since tin does not have a layered structure similar to graphite, it is difficult to obtain stanene by using the mechanical stripping method. Instead, it can be prepared by using the molecular beam epitaxy method [5]. However, stanene nanoribbons need to be passivated before being used in devices. As a requisite step in the material preparation as well as device fabrication [10–12], passivation is an effective strategy for suppressing defect formation [13–16]. *In situ* angle-resolved photoemission spectroscopy together with first-principles calculations reveal an automatic passivation of the  $p_z$  orbital of the stanene [17]. Hydrogen passivation as a surfactant plays an important role in boosting the growth of stanene multilayers and improving the overall quality of stanene films [6].

Meanwhile, passivation is also critical for materials with surface-sensitive natures, such as silicene nanoribbons [18], halide perovskites [19], superconducting transmon qubits [20], and black phosphorus [21]. The effect of passivating atoms on electronic properties and band engineering of two-dimensional materials has attracted great attention in, e.g., graphene [22–25] and silicene systems [26–28].

Moreover, by calculating the formation energy and band gap of passivated zigzag stanene nanoribbons (ZSNRs), both hydrogen and fluorine passivation can increase the stability of ZSNRs and change their band gap [29,30]. The edge states and Dirac cones of ZSNRs can be significantly altered for the passivation of different elements [31]. In addition, one can effectively modulate the band structures and transport properties by utilizing the electric field [32], strain [33], exchange fields [34], boundaries [35,36], and disorder [37]. High-quality stanene films present the coexistence of nontrivial topology and intrinsic superconductivity. Passivation as a surfactant plays an important role in improving the overall quality of stanene films, and can significantly affect the edge states. However, clear and solid evidence of the edge states modulated by passivating atoms remains elusive. Thus, in this paper, we study the transport properties of ZSNRs by considering the combined effect of the edge passivation, electric fields, and exchange fields.

The paper is organized as follows: In Sec. II, we introduce the nonequilibrium Green's function method (NEGF) to study the transport properties of ZSNRs. In Sec. III, we calculate the band structure and conductance of ZSNRs under the effect of edge passivation, electric fields and exchange fields. Finally, a summary is given in Sec. IV.

**II. THEORETICAL MODEL**

We utilize the four-band tight-binding model to describe the combined effect of the passivation, electric fields and exchange fields. The corresponding Hamiltonian can be written

\*Contact author: liyuan@hdu.edu.cn

†Contact author: xug@hdu.edu.cn

‡Contact author: wmliu@iphy.ac.cn

TABLE I. Hopping parameters of the stanene nanoribbon with different passivating atoms. The unit is eV.

Passivation	$t_1$	$t_2$	$t_3$	$\Delta V$
H	0.78	0.009	0.57	-2.321
Na	0.77	0.003	0.72	1.426
F	0.75	0.009	1.35	-6.899

as [31,38]

$$\begin{aligned}
H_{\text{TB}} = & t_1 \sum_{(i,j),\alpha} c_{i,\alpha}^\dagger c_{j,\alpha} + it_2 \sum_{\langle\langle i,j \rangle\rangle,\alpha,\beta} v_{ij} c_{i,\alpha}^\dagger s_{\alpha\beta}^z c_{j,\beta} \\
& + \Delta V \sum_{\ell,\alpha} d_{\ell,\alpha}^\dagger d_{\ell,\alpha} + t_3 \sum_{(i,\ell),\alpha} c_{i,\alpha}^\dagger d_{\ell,\alpha} \\
& + \sum_{i,\alpha} eL_z E_{z1/z2} \xi_i c_{i\alpha}^\dagger c_{i\alpha} + \sum_{i,\alpha} M s_z c_{i\alpha}^\dagger c_{i\alpha} + \text{H.c.}, \quad (1)
\end{aligned}$$

where H.c. stands for Hermitian conjugate,  $c_{i,\alpha}^\dagger$  ( $c_{j,\beta}$ ) and  $d_{\ell,\alpha}^\dagger$  ( $d_{\ell,\beta}$ ) are the creation (annihilation) operators of tin atoms and passivating atoms, respectively, with spin index  $\alpha$  ( $\beta$ ) at sites  $i$ ,  $j$ , or  $\ell$ .  $\langle\langle i, j/\ell \rangle\rangle / \langle\langle i, j \rangle\rangle$  runs over all the nearest- or next-nearest-neighbor hopping sites with the hopping energy  $t_1/t_3$  or  $t_2$ .  $v_{ij} = \pm 1$  represents the anticlockwise (clockwise) hopping, and  $s_{\alpha\beta}^z$  is  $z$  component of spin vector.  $\Delta V$  is the on-site potential defined as the difference between the work functions of a tin atom and the passivating atom.  $t_3$  denotes the interaction between tin and passivating atoms. The fifth term describes the contribution of the vertical electric field with  $U_{E,z1/z2} = eL_z E_{z1/z2}$  and  $L_z = 0.84 \text{ \AA}$  being the distance of the two sublattice planes [9] with  $\xi_i = \pm 1$  for A (B) sites, where  $z1$  and  $z2$  distinguish two edge electric fields. The last term describes the contribution of the ferromagnetic exchange field with  $M$  being the magnetization and  $s_z = \pm 1$ .

Four parameters,  $t_{1,2,3}$  and  $\Delta V$ , were obtained by fitting the tight-binding model to the results of density functional theory (DFT) [31]. For the nonpassivated case, hopping parameters are chosen as  $t_1 = 0.76$ ,  $t_2 = 0.01$ ,  $t_3 = 0$ , and  $\Delta V = 0$ . We analyze the effect of three elements, hydrogen, sodium, and fluorine, on the transport properties of stanene nanoribbons. The hopping parameters of the passivated region are listed in Table I.

The conductance can be calculated by using the NEGF method and the Landauer-Büttiker formula [39,40]

$$G = \frac{e^2}{h} \text{Tr}[\Gamma_L G^r \Gamma_R G^a], \quad (2)$$

where  $\Gamma_{L/R} = i(\Sigma_{L/R}^r - \Sigma_{L/R}^a)$  are the linewidth functions and  $\Sigma_{L/R}^{r/a}$  is the retarded/advanced self energy, which can be obtained by iterating the semi-infinite lead. Then we can obtain the retarded and advanced Green's functions:

$$G^r = [G^a]^\dagger = [EI + i\eta - H_c - \Sigma_L^r - \Sigma_R^r]^{-1}, \quad (3)$$

where  $H_c$  is the Hamiltonian of the central scattering region. The density of states (DOS) of the system can be calculated by using the equation

$$\text{DOS} = -\frac{1}{\pi} \text{Im}(\text{Tr}[G^r]). \quad (4)$$

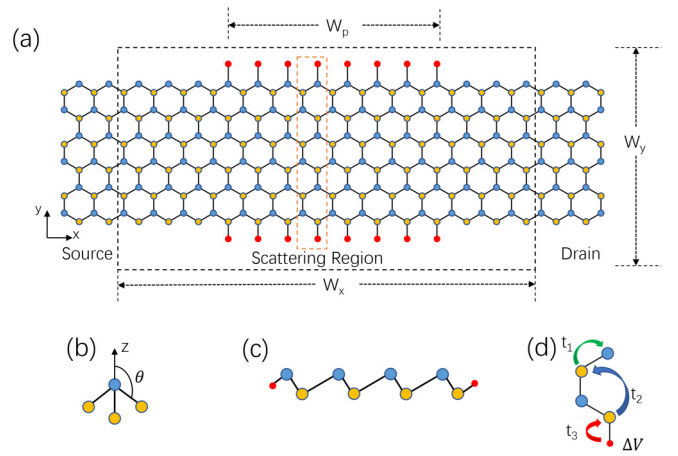


FIG. 1. (a) Schematic of the zigzag stanene nanoribbon with passivating atom (red). The blue and yellow sites represent the A and B sublattices of stanene, respectively. The orange dashed box refers to the unit cell.  $W_x$  and  $W_y$  represent the length and width of the scattering region.  $W_p$  refers to the length of the passivated region. (b)  $\theta$  is the angle between Sn-Sn bonds and the  $z$  axis. (c) The side view of the low-buckled stanene structure. (d) The hopping terms in ZSNRs with passivation.

### III. NUMERICAL RESULTS AND DISCUSSION

Figure 1 shows the schematic of ZSNRs, with  $W_x$  and  $W_y$  denoting the length and width of the nanoribbon, respectively. The length of the passivated part is  $W_p$ . The length  $W_x = [(N_x - 1)/2] \times \sqrt{3}a_0$ , the width  $W_y = [(3N_y/4 - 1)] \times a_0$ , and the length of the passivated part  $W_p = [(2N_p - 1)/2] \times \sqrt{3}a_0$ , where  $a_0 = 0.283 \text{ nm}$  is the distance of two nearest tin atoms in the pristine region [9].  $N_x$  and  $N_y$  are the numbers of sites along the  $x$  and  $y$  directions of the nanoribbon, and  $N_p$  is the number of passivating sites in the edge of the nanoribbon. One can realize the edge passivation in experiments by adopting initiated chemical vapor deposition [11], bilateral passivation strategy [12], atomic layer deposition method [41], and so on.

#### A. Band bending and the passivation-modulated conductance

We first consider the effect of passivation on the band structure of ZSNRs. In the absence of any passivation, as shown in Fig. 2(a), the edge bands exhibit linear dispersion relations, which is a quantum spin-Hall edge state. For the system with passivation, dangling bonds are replaced by the passivation bonds, and the edge bands become bent [31]. Moreover, the distortion direction and the amplitude of the edge bands significantly depend on the electronegativity difference between the passivating atoms and tin atoms. The electronegativity of atoms lead to the increase of the hopping energy between atoms. Correspondingly, the energies of the edge bands bending upwards are relatively high compared to the case without passivation. The electronegativity of the fluorine atoms is larger than that of the hydrogen atoms, and the hopping energies between fluorine atoms and tin atoms are relatively stronger. Thus the degree of distortion of the edge bands of the fluorine-passivated nanoribbon is larger

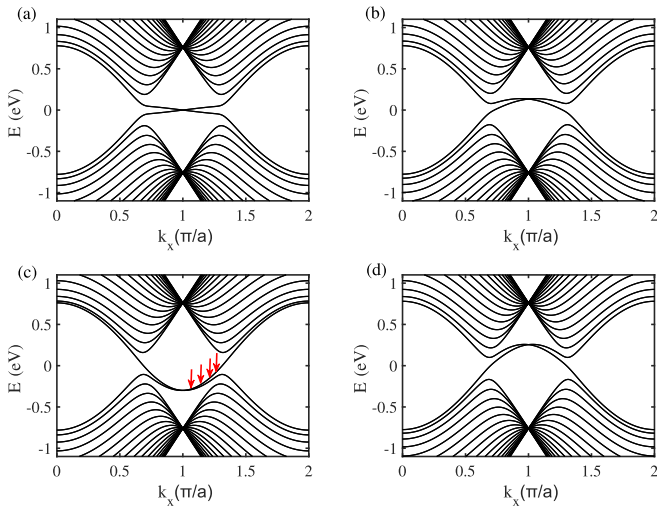


FIG. 2. Band structures of different passivated systems: (a) non-passivated ZSNRs, (b) H-passivated ZSNRs, (c) Na-passivated ZSNRs, (d) F-passivated ZSNRs with  $N_y = 36$ . The probability density of the energy band marked by red arrows was calculated.

than that of the hydrogen-passivated nanoribbon, as shown in Figs. 2(b) and 2(d). Since sodium is electropositive compared to tin, the edge bands of the sodium-passivated nanoribbon bend downwards as opposed to the upward bending in the hydrogen-passivated and fluorine-passivated nanoribbons [see Fig. 2(c)]. The physical mechanism of the band bending can be understood by means of the wave function of the edge state. Figure 3 plots the probability density  $|\Psi|^2$  of edge states as a function of the atom positions along the transverse direction of the Na-passivated ZSNRs, where the first and 38th atoms represent passivating atoms. Four wave vectors denoted by red arrows in Fig. 2(c),  $k_x = 1.0\pi/a$ ,  $1.1\pi/a$ ,  $1.2\pi/a$  and  $1.3\pi/a$ , are chosen to show the probability density. It can be seen that the states at symmetric point  $k_{xc} = 1.0\pi/a$  are localized only at the edges. With increase of  $k_x$ , the distribution of states gradually extend to the whole nanoribbon. The change in potential energy of the upper and lower edges is relatively larger due to the effect of the passivating atoms. For the state near  $k_{xc}$ , the major contribution of the wave

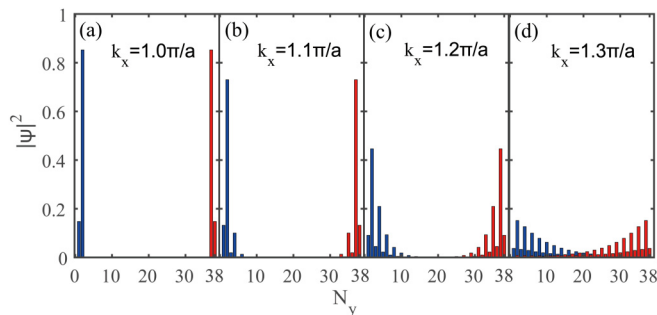


FIG. 3. The probability density  $|\Psi|^2$  for the wave functions of the edge states labeled by the red arrows in Fig. 2(c), where the blue and red lines are the states at the upper and lower boundaries of the nanoribbon, respectively. (a)  $k_x = 1.0\pi/a$ ; (b)  $k_x = 1.1\pi/a$ ; (c)  $k_x = 1.2\pi/a$ ; (d)  $k_x = 1.3\pi/a$ .

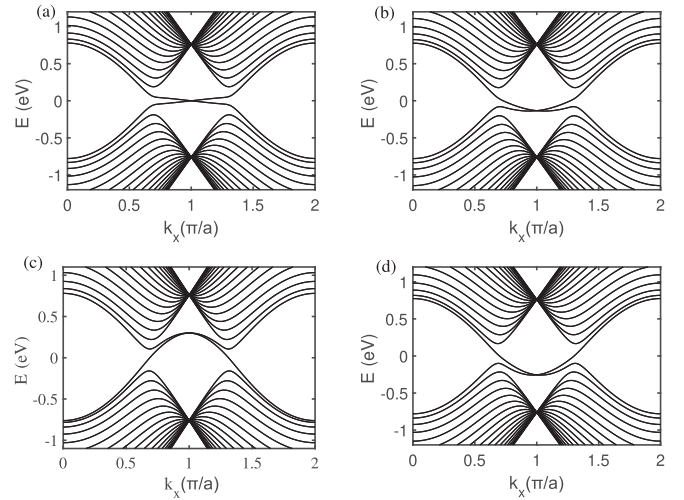


FIG. 4. Band structures of the passivated ZSNRs with  $N_y = 36$  for different on-site potentials: (a) non-passivated ZSNRs, (b)  $\Delta V = 2.321$ , (c)  $\Delta V = -1.426$ , (d)  $\Delta V = 6.899$ .

function comes from the atoms of the upper and lower edges. For states far from  $k_{xc}$ , the contribution comes from the entire nanoribbon. Thus, adding sodium atoms to the edges makes the edge energy bands near  $k_{xc}$  bend downwards obviously, while the bands far from  $k_{xc}$  have a small change and bend slightly. As a result, the bending amplitude of the edge energy band has a relative larger value.

In terms of the above analyses, it is found that the distortion direction and amplitude of the edge bands depend on the on-site potential, namely the electronegativity difference between the tin atoms and passivating atoms. In order to further verify this conclusion, we obtain the band structures of the passivated ZSNRs for different on-site potentials, as shown in Fig. 4. When  $\Delta V = 2.321$ , which is an opposite value of the on-site potential of the hydrogen-passivated ZSNRs, the edge bands bend downwards as opposed to the upward bending in the hydrogen-passivated nanoribbon, while the distortion amplitude is identical. Similarly, when  $\Delta V = -1.426$  and  $\Delta V = 6.899$ , we can obtain the opposite distortion behaviors of the edge bands compared to those of Na-passivated and F-passivated ZSNRs, respectively [see Figs. 4(c) and 4(d)]. That is to say, the on-site potential can be utilized to modulate the edge bands. Certainly, when the definition of the on-site potential is changed to the opposite value, namely the difference between the work functions of a passivating atom and the tin atom, one can also find the opposite distortion behaviors for the edge bands.

In line with the band bending, the influence of the passivating atoms can also be seen from the transport properties of ZSNRs, as shown in Fig. 5. In the absence of passivating atoms, there exist clear symmetrical conductance plateaus. The conductance plateau in the energy range of  $-0.2 < E < 0.2$  eV arises from the contribution of the edge bands. For the H-passivated ZSNRs, conductance dips occur within the lowest plateau [see Fig. 5(b)]. The energy range of  $0.03 < E < 0.12$  eV shows the shift of edge bands induced by the passivating hydrogen atoms. There are also small oscillating peaks near the plateaus rims. For Na-passivated ZSNRs, as

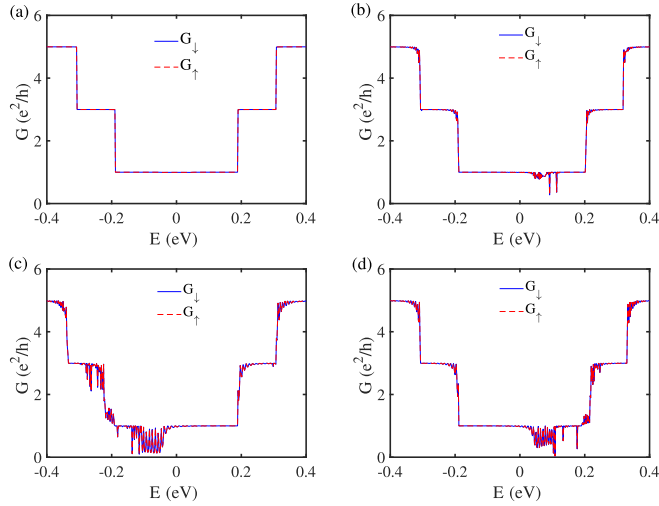


FIG. 5. Conductance is plotted as a function of the Fermi energy for different passivated systems: (a) nonpassivated ZSNRs; (b) H-passivated ZSNRs; (c) Na-passivated ZSNRs; (d) F-passivated ZSNRs. The parameters are set as  $N_x = 300$ ,  $N_y = 36$ , and  $N_p = 150$ . The arrows  $\uparrow$  and  $\downarrow$  refer to the spin-up and spin-down states, respectively.

shown in Fig. 5(c), the electropositivity of passivating Na atoms leads to the downward bending of edge bands, thus inducing significant conductance dips within the energy range of  $-0.19 < E < 0$  eV. Last, for the F-passivated ZSNRs [see Fig. 5(d)], the conductance dips move to the energy range of  $0 < E < 0.16$  eV, which also shows the upward shift of edge bands. When the on-site potential is changed to an opposite value, for example  $\Delta V = -1.426$  [see Fig. 4(c)], the upward-bending edge bands induce conductance dips within the energy range of  $0 < E < 0.19$  eV, which is a shift opposite to that of Na-passivated ZSNRs given in Fig. 5(c). Similarly, the conductance dips for the ZSNRs with  $\Delta V = 2.321$  and  $\Delta V = 6.899$  also occur at energy ranges opposite to those of the H-passivated and F-passivated ZSNRs. Even though the on-site potentials change signs, the band structure and the conductance peaks are basically identical except in the opposite distortion direction and energy range. Obviously, the conductance dips reflect the effect of passivating atoms on the edge states, which can be used to detect the edge states or the passivating atoms. The above results mean that the conductance dips act as fingerprints of the edge states or the passivating atoms.

In order to clearly understand the dependent relations and the effect of the passivation, we plot the band spectra and the corresponding conductance of Na-passivated ZSNRs in Fig. 6. In the energy range of  $-0.19 < E < 0$  eV, there are two modes of resonance peaks in the conductance. When  $-0.19 < E < -0.11$  eV, several downward resonance peaks occur, and the peak values tend to 0. This phenomenon can be understood based on the band-selective rule [42]. The energy bands of the center passivated region and two leads are given in Fig. 6(a), where the band index is specified. The electrons in the even (odd) bands can be scattered only into the even (odd) bands due to the conservation of the parity of wave functions [43,44]. The highest valence band and the

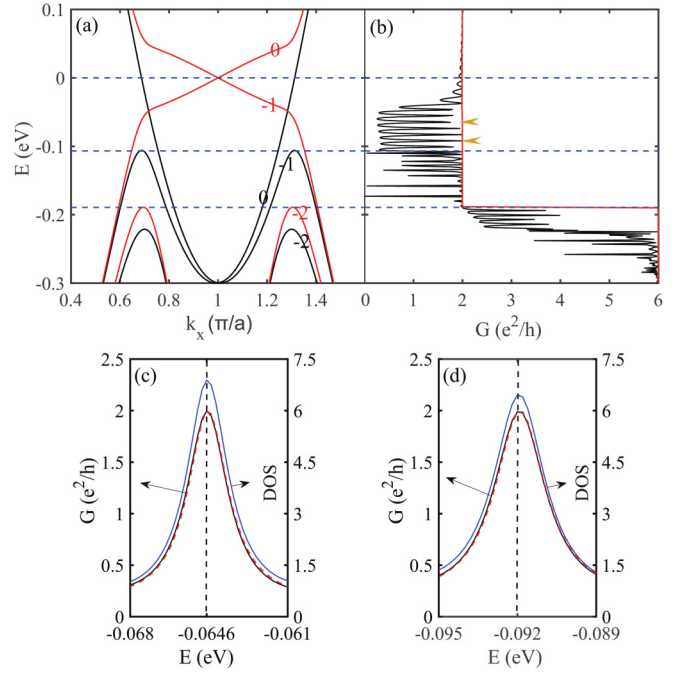


FIG. 6. (a)–(b) The band structure and conductance of Na-passivated ZSNRs; The red curves refer to the results of the pristine ZSNRs like the left and right leads. (c)–(d) The Fano resonance peaks marked in (b) are obtained by using NEGF (black curves) and fitted by the normalized Fano curve (red dashed curves). The blue curves refer to DOS corresponding to the Fano resonance peaks. Other parameters are the same as those given in Fig. 5.

lowest conduction band coexist in the band-bending region. In the center region, bands 0 and  $-1$  coexist at  $-0.19 < E < -0.11$  eV. In the left and right leads, only band  $-1$  exists at this energy range. Therefore, when an electron with energy  $E \in [-0.19, -0.11]$  eV passes through the system, if the electron of band  $-1$  in the lead is scattered into band  $-1$  of the center region, the conductance  $G$  is usually  $2e^2/h$  (spin degeneracy) and the plateau arises from nonresonant electron transmission. In contrast, if the electron of band  $-1$  in the lead is scattered into band 0 of center region, the conductance would drop to zero due to the opposite parities between the two bands, which results in conductance dips with small values. When  $-0.11 < E < 0$  eV, the electron of band  $-1$  in the lead can only be scattered into band 0 of the center region, which does not satisfy the parity conservation. In this case, the conductance should become zero in terms of the band-selective rule [35]. However, there exists an extraordinary phenomenon that some resonance peaks occur within the energy range of  $-0.11 < E < 0$  eV, which can be explained as the quantum spin-Hall edge state in the leads preventing the backscattering of electrons. When the hopping parameter  $t_2$  decreases to a certain value, for example  $t_2 = 0.001$  eV, the quantum spin-Hall edge state changes to a flat band. Correspondingly, the conductance peaks within  $-0.11 < E < 0$  eV evolve into a zero-conductance plateaus. Obviously, the conductance peaks can also act as fingerprints of the quantum spin-Hall edge states.

The resonance behavior of the conductance can be described by the Fano resonance. The asymmetric line shapes

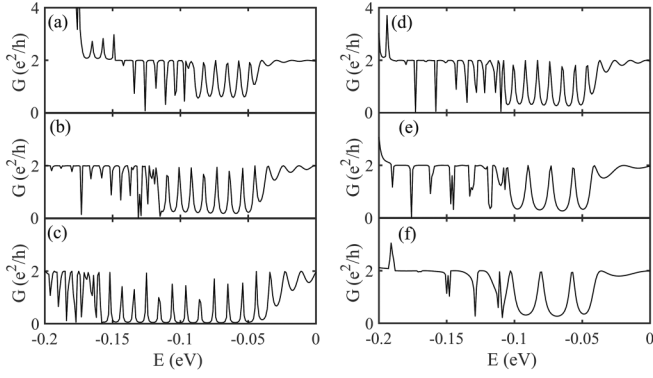


FIG. 7. Conductance of Na-passivated ZSNRs is plotted as a function of Fermi energy for different transverse widths and passivated regions: (a)  $N_y = 48$ ,  $N_p = 150$ ; (b)  $N_y = 32$ ,  $N_p = 150$ ; (c)  $N_y = 20$ ,  $N_p = 150$ ; (d)  $N_y = 36$ ,  $N_p = 150$ ; (e)  $N_y = 36$ ,  $N_p = 75$ ; (f)  $N_y = 36$ ,  $N_p = 50$ .

of the Fano resonance can be expressed as [45]

$$T(E) = \frac{T_0}{1+q^2} \frac{(\epsilon + q^2)}{1 + \epsilon^2}, \quad (5)$$

with  $\epsilon = (E - E_F)/\gamma$ .  $E_F$  and  $\gamma$  determine the position and width of the Fano curve, respectively.  $T_0$  is the maximum value of the peak, which depends on the magnitude of the resonance. The asymmetry parameter  $q$  gives the ratio of the transition probability of the mixed state to that of the continuum, which is a fitting parameter and determines the shape of the Fano curve. The Fano resonance curves are calculated in terms of Eq. (5), which associates with the conductance curves labeled by the yellow triangles in Fig. 6(b). The parameters of the two Fano curves in Figs. 6(c) and 6(d) are set as  $T_0 = 1.855$ ,  $q = 200$ ,  $\gamma = 0.00114$ . The positions of the corresponding DOS peaks match very well with peaks of the Fano resonances. It means that the conductance dips induced by passivating atoms can be understood in terms of the physical mechanism of the Fano resonance.

Next, we investigate the finite size effect of the nanoribbon on the transport properties. We plot the conductance of ZSNRs for different transverse widths and passivated regions in the energy range  $-0.2 < E < 0$  eV. In Figs. 7(a)–7(c), the transverse sites  $N_y$  of ZSNRs are chosen as 48, 32, and 20, respectively. The number of passivated sites is fixed to  $N_p = N_x = 150$ . With decreasing transverse width, the amplitude and frequency of the resonance increase. This means that the Fano resonance becomes stronger for smaller nanoribbons due to the interferometric effect. In Figs. 7(d)–7(f), the transverse width is fixed to  $N_y = 36$ , and the width of the passivated region  $N_p$  changes from 150 to 50. Obviously, the resonance frequency gradually decreases with decreasing passivated width. It means that the edge passivation atoms can significantly affect the Fano resonance.

Next we analyze the effect of the disorder on the conductance. The on-site disorder  $\sum_{i,\alpha} \Omega_i c_{i\alpha}^\dagger c_{i\alpha}$  is introduced into the Hamiltonian, which is uniformly distributed within  $[-\Omega/2, \Omega/2]$  with  $\Omega$  representing the disorder strength. For the nonpassivated ZSNRs, as shown in Fig. 8(a), the conductance gradually decreases and the plateaus are destroyed by the

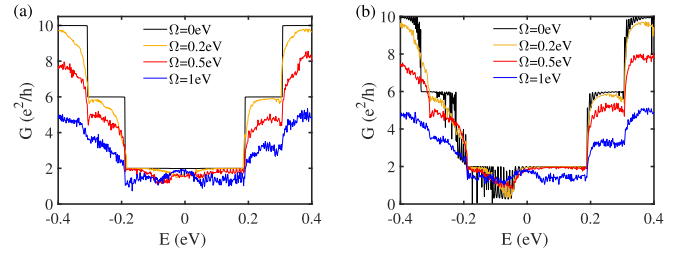


FIG. 8. Conductance is plotted as a function of the Fermi energy for different disorder strengths: (a) nonpassivated ZSNRs; (b) Na-passivated ZSNRs. Other parameters are the same as those given in Fig. 5.

disorder strength  $\Omega$  increases from 0.2 to 1 eV. Similarly, the conductance plateaus are also destroyed by the disorder for the Na-passivated ZSNRs. However, one can find the oscillating peaks within the energy range  $-0.2 < E < 0$  eV, which can still be regarded as the characteristics of passivating atoms.

In the following, we analyze double atom passivation [46]: The upper edge is passivated by fluorine atoms and the lower one is passivated by sodium atoms (see Fig. 9). Since the passivating atoms on the upper and lower edges have different electronegativities relative to tin atoms, one of the edge bands bends upwards, while the other edge band bends downwards. In addition, the edge bands are asymmetrical about the axis  $k_{xc}$  and a band gap about 0.08 eV is opened. Especially, the asymmetrical passivation induces spin-valley dependent edge bands. As shown in Fig. 9(b), the conductance has a zero value in the energy range of  $-0.0338 < E < 0.0138$  eV associated with the band gap. Though the edge bands are spin-valley dependent, the total energy bands are still symmetrical about the axis  $k_{xc}$ . Thus the spin-up and spin-down conductances are identical.

### B. Combined effects of the passivation, the edge electric field and the exchange field

We first study the effect of edge electric fields on the band structure and the transport properties of ZSNRs in the absence of passivating atoms. As shown in Fig. 10(a), two vertical electric fields,  $E_{z1}$  and  $E_{z2}$ , are applied to the upper and lower edges of ZSNRs. The width and strength of the electric fields are denoted by  $W$  and  $U_{E,z1/z2}$ , respectively.

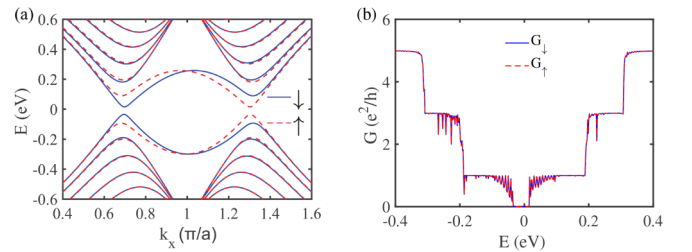


FIG. 9. (a) The band structure of ZSNRs with double atom passivation, i.e., fluorine and sodium atoms. (b) The conductance as a function of Fermi energy. The parameters are set as  $N_x = 300$ ,  $N_y = 36$ , and  $N_p = 150$ .

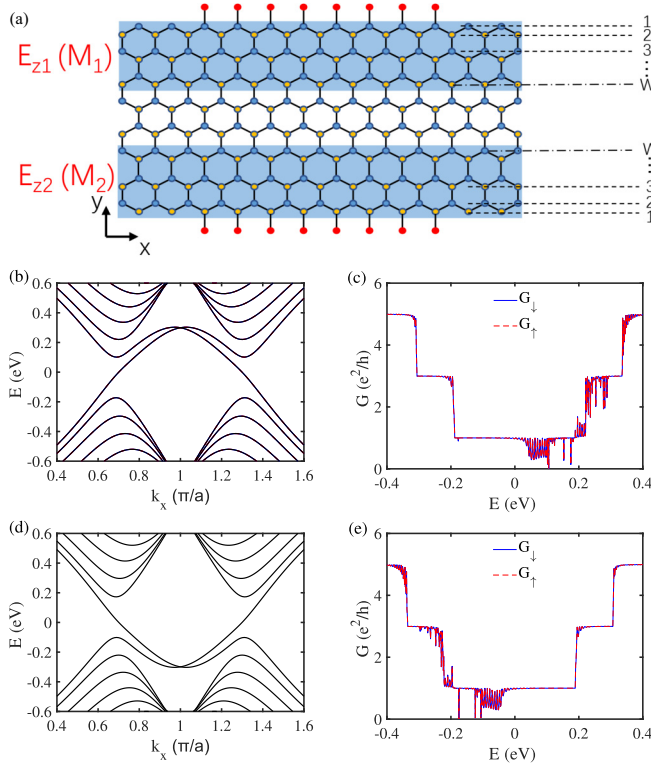


FIG. 10. The schematic diagram of ZSNRs applied with two electric fields  $E_{z1}$  and  $E_{z2}$  on the edges of the nanoribbon, with  $W$  referring to the width of the electric fields. The band structure and the corresponding conductance for the cases (b)–(c)  $U_{E,z1} = -U_{E,z2} = 0.3$  eV and (d)–(e)  $U_{E,z1} = -U_{E,z2} = -0.3$  eV with the width  $W = 2$ . The parameters are set as  $N_x = 300$ ,  $N_y = 36$ , and  $N_p = 0$ .

We plot the band structure and the conductance of ZSNRs for the case  $U_{E,z1} = -U_{E,z2} = 0.3$  eV and  $W = 2$  [Figs. 10(b)–10(c)]. The edge bands bend upwards due to the effect of the electric fields, which are similar to those induced by the passivating fluorine atoms [see Fig. 2(d)]. Correspondingly, there also exist some resonance peaks of the conductance in the energy range of  $0 < E < 0.3$  eV, which can be detected as the characteristic of the edge states. When the electric fields are changed to  $U_{E,z1} = -U_{E,z2} = -0.3$  eV, the edge bands bend downwards, which is different from the former case and similar to that induced by the passivating sodium atoms. The resonance peaks of the conductance change to the energy range of  $-0.3 < E < 0$  eV. It means that the edge antisymmetric electric fields can be used to modulate the bending edge bands, interestingly, which can recover the passivation-induced band structures and the transport properties.

In order to analyze the combined effect of the passivating atoms and the edge electric fields, we further study the band structure and conductance of ZSNRs applied with the edge antisymmetric electric fields  $U_{E,z1} = -U_{E,z2} = 0.36$  eV and passivating Na atoms, as shown in Fig. 11. Compared with Fig. 2(c), the curved edge bands arising from the passivation have completely disappeared. The resonance peaks of the conductance also disappear. Under the combined action of the edge passivation and asymmetric electric fields, the

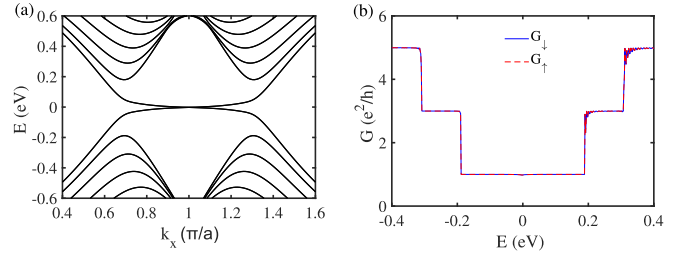


FIG. 11. The band structure and the corresponding conductance of ZSNRs with Na passivation and edge electric fields. The parameters are set as  $U_{E,z1} = -U_{E,z2} = 0.36$  eV,  $N_p = 150$ , and  $W = 2$ .

energy bands and conductance behaviors of ZSNRs gradually approach the case of the pristine ZSNRs. Therefore, we can apply the edge asymmetric electric fields to simulate or modulate the effect of edge passivation on ZSNRs. Similarly, the effect of edge asymmetric electric fields can be simulated by adsorbing different atoms to the edges of ZSNRs. Nowadays, monolayer stanene can be prepared by molecular beam epitaxy growth, and usually has passivating atoms attached to the edges. Edge passivation plays an important role in the structural stability of stanene. So if the edge electric fields can be used to simulate or modulate the effect of the edge passivation on energy bands and conductance, it will be of great help for the study and application of stanene systems.

Next, we analyze the effect of the edge symmetric electric fields on the transport properties of ZSNRs. The electric field is set as  $U_{E,z1} = U_{E,z2} = 0.3$  eV, as shown in Fig. 12. Since the sublattices of the upper and lower edges of the ZSNRs are different, the potential at the A (B) sublattice on the upper (lower) edge is positive (negative) when  $U_{E,z1} = U_{E,z2} = 0.3$  eV. Thus, the staggered sublattice potentials between A and B sublattices on the edges would separate the edge energy band and thus open a band gap, which is similar to the phenomenon induced by double atom passivation. And the edge symmetric electric fields also lead to spin-valley polarization.

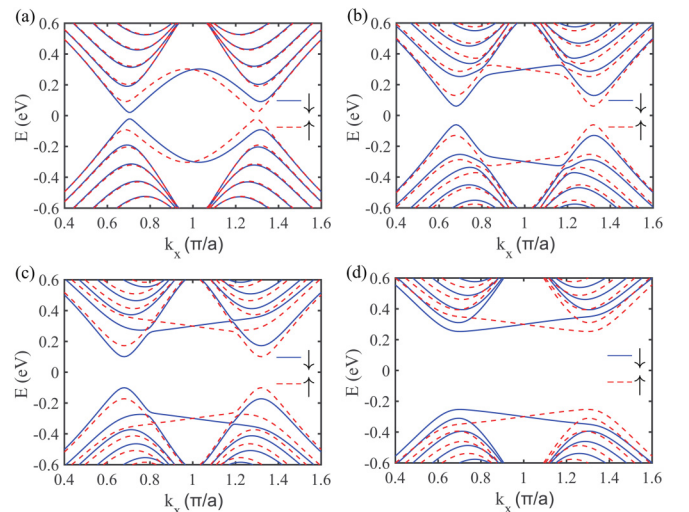


FIG. 12. The band structure of ZSNRs with symmetrical electric fields  $U_{E,z1} = U_{E,z2} = 0.3$  eV for different widths (a)  $W = 2$ , (b)  $W = 8$ , (c)  $W = 12$ , and (d)  $W = 18$ .

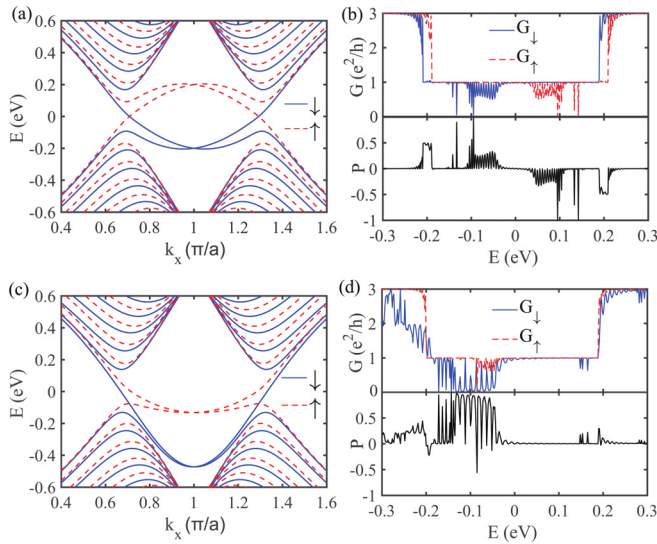


FIG. 13. The band structure, conductance and spin polarization for (a)–(b) nonpassivated ZSNRs and (c)–(d) Na-passivated ZSNRs. The parameters are set as  $M_1 = M_2 = 0.2$  eV,  $N_x = 300$ ,  $N_y = 36$ ,  $N_p = 150$ , and  $W = 2$ .

Interestingly, the amplitude of the band gap depends on the width  $W$  of the electric field. As the width  $W$  increases from 2 to 18, the band gap significantly increases from 0.08 eV to about 0.45 eV [see Figs. 12(a)–12(d)]. When the symmetrical electric fields are extended over the entire nanoribbon ( $W = N_y/2 = 18$ ), the band gap reaches its maximum value.

The exchange field is crucial for spin-based devices to realize an effective modulation of spin polarization. Thus we further study the combined effect of the exchange field  $M$  and the passivating atoms on the transport properties of ZSNRs. First, the exchange field is also applied on the edges of ZSNRs. We plot the band structure, conductance, and spin polarization in Fig. 13 for  $M_1 = M_2 = 0.2$  eV. The spin polarization is defined as  $P = (G_\uparrow - G_\downarrow)/(G_\uparrow + G_\downarrow)$  [34]. The spin-up edge band bends upwards, while the spin-down edge band bends downwards. Simultaneously, the spin-dependent edge bands result in the resonance peaks of the conductance moving towards opposite directions. Correspondingly, the spin polarization also exhibits some resonance peaks, which are associated with the spin-dependent conductance given in Fig. 13(b). The variation of the edge states can be detected in terms of the spin-dependent conductance and spin polarization. We can see in Figs. 13(c)–13(d) that, under the combined action of the passivation and edge exchange fields, both of spin-up and spin-down edge bands move downwards. The spin-down edge bands significantly bend downwards, while the spin-up edge bands gradually become flat. The

spin-dependent conductance peaks overlap with each other, thus inducing some significant oscillating peaks of spin polarization within the energy range of  $-0.2 < E < 0$  eV. Therefore, one can realize an effective spin polarization by applying an exchange field on the edges of ZSNRs.

According to the above analyses, one can propose a stanene-based device to detect the existence of the passivating atoms or the quantum spin-Hall edge state in terms of the characteristic of the conductance resonance peaks. If the quantum spin-Hall edge states in leads is modulated to flat edge bands by changing the hopping parameters, the conductance resonance peaks can evolve into zero conductance. At the same time, by applying an edge electric field, one can enhance or decrease the effect of the passivating atoms, and can open a band gap and obtain zero-conductance behaviors. The exchange fields can further induce spin-polarized transport. Thus a stanene-based device can realize multiple ways to effectively modulate the system's transport properties.

#### IV. CONCLUSIONS

In summary, we have systematically studied the band structure, conductance, and spin polarization modulated by the passivation, edge electric fields and exchange fields in ZSNRs by using the NEGF method. In the absence of passivating atoms, the edge bands of ZSNRs exhibit linear dispersion relations, which is a quantum spin-Hall edge state. For the edge passivation case, the curved direction and amplitude of edge bands significantly depend on the electronegativity difference between the passivating atoms and tin atoms. The conductance dips can reflect the characteristic of the curved bands induced by passivating atoms, which can be used to detect the quantum spin-Hall edge states or passivating atoms. The edge asymmetric electric fields can simulate or modulate the curved edge bands and recover the passivation-induced transport properties, while the edge symmetric electric fields can separate edge bands and open a band gap, and induce a spin-valley polarization. The exchange fields on the edges of ZSNRs can induce a spin-dependent conductance and an effective spin polarization. Our results shed light on the promising application of the passivation effect based on stanene devices in nanoelectronics and spintronics.

#### ACKNOWLEDGMENTS

This work was supported by National Key R&D Program of China under Grants No. 2021YFA1400900, No. 2021YFA0718300 and No. 2021YFA1402100, by the NSFC under Grants No. 52327808, No. 11574067, No. 12174461, No. 12234012, and No. 12334012, by the Space Application System of China Manned Space Program, and by the Natural Science Foundation of Zhejiang Province (Grant No. LTGS24E060005).

- [1] M. J. Gilbert, Topological electronics, *Commun. Phys.* **4**, 70 (2021).  
 [2] M. He, H. Sun, and Q. L. He, Topological insulator: Spintronics and quantum computations, *Front. Phys.* **14**, 43401 (2019).

- [3] S. Balendhran, S. Walia, H. Nili, S. Sriam, and M. Bhaskaran, Elemental analogues of graphene: Silicene, germanene, stanene, and phosphorene, *Small* **11**, 640 (2015).  
 [4] Y. Xu, B. Yan, H. J. Zhang, J. Wang, G. Xu, P. Z. Tang, W. H. Duan, and S. C. Zhang, Large-gap quantum spin

- Hall insulators in tin films, *Phys. Rev. Lett.* **111**, 136804 (2013).
- [5] F. F. Zhu, W. J. Chen, Y. Xu, C. L. Gao, D. D. Guan, C. H. Liu, D. Qian, S. C. Zhang, and J. F. Jia, Epitaxial growth of two-dimensional stanene, *Nat. Mater.* **14**, 1020 (2015).
- [6] C. Zhao, L. Li, L. Zhang, J. Qin, H. Chen, B. Xia, B. Yang, H. Zheng, S. Wang, C. Liu, Y. Li, D. Guan, P. Cui, Z. Zhang, and J. Jia, Coexistence of robust edge states and superconductivity in few-layer stanene, *Phys. Rev. Lett.* **128**, 206802 (2022).
- [7] S. C. Wu, G. C. Shan, and B. H. Yan, Prediction of near-room-temperature quantum anomalous Hall effect on honeycomb materials, *Phys. Rev. Lett.* **113**, 256401 (2014).
- [8] J. Wang, Y. Xu, and S. C. Zhang, Two-dimensional time-reversal-invariant topological superconductivity in a doped quantum spin-Hall insulator, *Phys. Rev. B* **90**, 054503 (2014).
- [9] J. K. Lyu, S. F. Zhang, C. W. Zhang, and P. J. Wang, Stanene: A promising material for new electronic and spintronic applications, *Ann Phys. (NY)* **531**, 1900017 (2019).
- [10] M. Lang, L. He, F. Xiu, X. Yu, J. Tang, Y. Wang, X. Kou, W. Jiang, A. V. Fedorov, and K. L. Wang, Revelation of topological surface states in Bi<sub>2</sub>Se<sub>3</sub> thin films by *in situ* Al passivation, *ACS Nano* **6**, 295 (2012).
- [11] H. Park, J. Choi, J. Shim, S. M. Lee, S. On, H. J. Yun, S. Kim, S. G. Im, and H. Yoo, Functional polymeric passivation-led improvement of bias stress with long-term durability of edge-rich nanoporous MoS<sub>2</sub> thin-film transistors, *npj 2D Mater. Appl.* **6**, 21 (2022).
- [12] L. M. Xu, J. H. Li, B. Cai, J. Z. Song, F. J. Zhang, T. Fang, and H. B. Zeng, A bilateral interfacial passivation strategy promoting efficiency and stability of perovskite quantum dot light-emitting diodes, *Nat. Commun.* **11**, 3902 (2020).
- [13] L. Fu, H. Li, L. Wang, R. Yin, B. Li, and L. Yin, Defect passivation strategies in perovskites for an enhanced photovoltaic performance, *Energy Environ. Sci.* **13**, 4017 (2020).
- [14] F. Gao, Y. Zhao, X. W. Zhang, and J. B. You, Recent progresses on defect passivation toward efficient perovskite solar cells, *Adv. Energy Mater.* **10**, 1902650 (2020).
- [15] H. Kim, K. Nam, J. Park, M. Kang, J. S. Bae, W. T. Hong, H. K. Yang, J. H. Jeong, J. H. Oh, and S. Lee, Hydrogen-mediated manipulation of luminescence color in single-component Eu doped CaYAlSiO<sub>4</sub> by defect passivation, *J. Alloys Compd.* **932**, 167610 (2023).
- [16] Y. Zhao, P. Zhu, S. Huang, S. Tan, M. Wang, R. Wang, J. Xue, T. H. Han, S. J. Lee, A. Zhang, T. Huang, P. Cheng, D. Meng, J. W. Lee, J. Marian, J. Zhu, and Y. Yang, Molecular interaction regulates the performance and longevity of defect passivation for metal halide perovskite solar cells, *J. Am. Chem. Soc.* **142**, 20071 (2020).
- [17] Y. Zang, T. Jiang, Y. Gong, Z. Guan, C. Liu, M. Liao, K. Zhu, Z. Li, L. Wang, W. Li, C. Song, D. Zhang, Y. Xu, K. He, X. Ma, S. C. Zhang, and Q. K. Xue, Realizing an epitaxial decorated stanene with an insulating bandgap, *Adv. Funct. Mater.* **28**, 1802723 (2018).
- [18] R. C. Junghare and G. C. Patil, Investigation of transport in edge passivated armchair silicene nanoribbon field effect transistor by *ab-initio* based Wannierised tight binding, *Superlattices Microstruct.* **156**, 106933 (2021).
- [19] X. D. Wang, Y. H. Huang, J. F. Liao, Z. F. Wei, W. G. Li, Y. F. Xu, H. Y. Chen, and D. B. Kuang, Surface passivated halide perovskite single-crystal for efficient photoelectrochemical synthesis of dimethoxydihydrofuran, *Nat. Commun.* **12**, 1202 (2021).
- [20] M. Mergenthaler, C. Müller, M. Ganzhorn, S. Paredes, P. Müller, G. Salis, V. P. Adiga, M. Brink, M. Sandberg, J. B. Hertzberg, S. Filipp, and A. Fuhrer, Effects of surface treatments on flux tunable transmon qubits, *npj Quantum Inf.* **7**, 157 (2021).
- [21] Y. Abate, D. Akinwande, S. Gamage, H. Wang, M. Snure, N. Poudel, and S. B. Cronin, Recent progress on stability and passivation of black phosphorus, *Adv. Mater.* **30**, 1704749 (2018).
- [22] Y. H. Lu, R. Q. Wu, L. Shen, M. Yang, and Z. D. Sha, Effects of edge passivation by hydrogen on electronic structure of armchair graphene nanoribbon and band gap engineering, *Appl. Phys. Lett.* **94**, 122111 (2009).
- [23] B. Mandal, S. Sarkar, A. Pramanik, and P. Sarkar, Electronic structure and transport properties of sulfur-passivated graphene nanoribbons, *J. Appl. Phys.* **112**, 113710 (2012).
- [24] P. Wagner, C. P. Ewels, J. J. Adjizian, L. Magaud, P. Pochet, S. Roche, A. L. Bezanilla, V. V. Ivanovskaya, A. Yaya, and M. Rayson, Band gap engineering via edge-functionalization of graphene nanoribbons, *J. Phys. Chem. C* **117**, 26790 (2013).
- [25] M. Yaghoobi Notash, A. Rastkar Ebrahimzadeh, J. Jahanbin Sardroodi, and B. Ghavami, Band gap tuning of hydrogen-and oxygen-passivated zigzag graphene monoxide nanoribbon: *Ab initio* computations, *Appl. Phys. A* **124**, 234 (2018).
- [26] M. Houssa, E. Scalise, K. Sankaran, G. Pourtois, V. V. Afanas'ev, Electronic properties of hydrogenated silicene and germanene, *Appl. Phys. Lett.* **98**, 223107 (2011).
- [27] N. Gao, W. T. Zheng, and Q. Jiang, Density functional theory calculations for two-dimensional silicene with halogen functionalization, *Phys. Chem. Chem. Phys.* **14**, 257 (2012).
- [28] R. Quhe, R. Fei, Q. Liu, J. Zheng, H. Li, C. Xu, Z. Ni, Y. Wang, D. Yu, Z. Gao, and J. Lu, Tunable and sizable band gap in silicene by surface adsorption, *Sci. Rep.* **2**, 853 (2012).
- [29] V. Nagarajan and R. Chandiramouli, Investigation of electronic properties and spin-orbit coupling effects on passivated stanene nanosheet: A first-principles study, *Superlattices Microstruct.* **107**, 118 (2017).
- [30] S. Kharwar, S. Singh, and B. K. Kaushik, Hydrogenated cove-edge aluminum nitride nanoribbons for ultrascaled resonant tunneling diode applications: a computational DFT study, *Nanotechnology* **34**, 245709 (2023).
- [31] E. Deylgat, S. Tiwari, and W. G. Vandenberghe, Impact of passivation on the Dirac cones of 2D topological insulators, *J. Appl. Phys.* **131**, 235101 (2022).
- [32] M. Ezawa, A topological insulator and helical zero mode in silicene under an inhomogeneous electric field, *New J. Phys.* **14**, 033003 (2012).
- [33] C. Si, J. Liu, Y. Xu, J. Wu, B. L. Gu, and W. Duan, Functionalized germanene as a prototype of large-gap two-dimensional topological insulators, *Phys. Rev. B* **89**, 115429 (2014).
- [34] L. H. Liao, Y. Ding, F. Wan, J. Y. Zhang, Z. H. Chen, X. Y. Cheng, R. Bai, G. F. Xu, and Y. Li, Switching modulation of spin transport in ferromagnetic tetragonal silicene, *Physica E* **147**, 115613 (2023).
- [35] W. T. Lu, Q. F. Sun, H. Y. Tian, B. H. Zhou, and H. M. Liu, Band bending and zero-conductance resonances controlled by



- edge electric fields in zigzag silicene nanoribbons, *Phys. Rev. B* **102**, 125426 (2020).
- [36] Z. Z. Zhang and K. Chang, Tuning of energy levels and optical properties of graphene quantum dots, *Phys. Rev. B* **77**, 235411 (2008).
- [37] A. Huang, S. Ke, J. H. Guan, and W. K. Lou, Tight-binding model and quantum transport with disorder for 1T' transition metal dichalcogenides, *J. Appl. Phys.* **134**, 084302 (2023).
- [38] C. L. Kane, and E. J. Mele,  $Z_2$  topological order and the quantum spin Hall effect, *Phys. Rev. Lett.* **95**, 146802 (2005).
- [39] M. Büttiker, Y. Imry, R. Landauer, and S. Pinhas, Generalized many-channel conductance formula with application to small rings, *Phys. Rev. B* **31**, 6207 (1985).
- [40] F. Wan, X. R. Wang, Y. W. Guo, J. Y. Zhang, Z. C. Wen, and Y. Li, Role of line defect in the bandgap and transport properties of silicene nanoribbons, *Phys. Rev. B* **104**, 195413 (2021).
- [41] N. Liu, J. Baek, S. M. Kim, S. Hong, Y. K. Hong, Y. S. Kim, H. S. Kim, S. Kim, and J. Park, Improving the stability of high-performance multilayer MoS<sub>2</sub> field-effect transistors, *ACS Appl. Mater. Interfaces* **9**, 42943 (2017).
- [42] J. Nakabayashi, D. Yamamoto, and S. Kurihara, Band-selective filter in a zigzag graphene nanoribbon, *Phys. Rev. Lett.* **102**, 066803 (2009).
- [43] A. Cresti, G. Grosso, and G. P. Parravicini, Valley-valve effect and even-odd chain parity in  $p$ - $n$  graphene junctions, *Phys. Rev. B* **77**, 233402 (2008).
- [44] J. C. Chen, S. G. Cheng, S. Q. Shen, and Q. F. Sun, Electronic transport through a graphene-based ferromagnetic/normal/ferromagnetic junction, *J. Phys.: Condens. Matter* **22**, 035301 (2010).
- [45] A. E. Miroshnichenko, S. Flach, and Y. S. Kivshar, Fano resonances in nanoscale structures, *Rev. Mod. Phys.* **82**, 2257 (2010).
- [46] H. L. Shi, M. R. Song, Z. T. Jiang, Y. H. Ren, and Q. Z. Han, Influence of edge passivation on the transport properties of the zigzag phosphorene nanoribbons, *Phys. Lett. A* **384**, 126486 (2020).